Advances in Astronautics Science and Technology (2022) 5:241–249
https://doi.org/10.1007/s42423-022-00124-6

ORIGINAL PAPER

Dynamic Analysis of Deployable Strut-Mechanism with Clearance Root-Joints for Spacial Flexible Solar Array

Shuli Yang[1] · **Limin Shao**[1] · **Yuhong Wang**[1]

Received: 21 February 2022 / Revised: 30 April 2022 / Accepted: 6 May 2022 / Published online: 28 June 2022

Abstract
With Kane dynamics theory, the multi-body dynamic models of deployable struts are established with considering the clearance root-joint and the deployable style and deployable process of the struts are studied. The dynamic performance of struts' deployment is analyzed, such as geometric position, velocity, and acceleration, seeking the inherent regularity of each joint's motion characteristics. The results show that root-joint's clearance has almost no influence on the rotation angle and angular velocity of base strut, but to some extent effect on the angular acceleration of base strut. Amplitude of angular acceleration appears significant fluctuations in 0–2 s and stabilizes gradually, indicating the pin in the bush is in the state of constant contact and separation. The dynamic model of deployable struts considering root-joint's clearance represents more realistically the dynamic characteristics of this system. The different hinges suffer different contact forces, and its impact how effects on the mechanism movement is different. Therefore, Analysis of the dynamic performance and design of deployable struts need to consider the impact of hinge clearance, which gain the motion characteristics of important parts during deploying process, providing guidance for future design of mechanisms and driving forces.

Keywords Spacial solar array · Deployable strut-mechanism with multiple bays · Clearance joint · Kane method

1 Introduction

Deployment mechanisms achieving folded or unfolded movement such as coilable mast, articulated mast, and pipe mast have been generally used in spacial flexible solar array. The truss which coilable mast becomes after deployment has obvious characteristics of nonlinearity; Deployment mechanism of articulated mast contains a lot of hinges, parts and more complicated folded mechanisms; and pipe mast has the relatively low stiffness and strength [1]. Multi-module deployable strut-mechanism of flexible solar array has been seen as a new type of deployable mechanism [2], having the advantages of low weight, high stiffness, low stowed volume, etc., which can be satisfied the requirements of accommodating other components such as flexible blankets and thin solar cells when stowed and providing the support and stiffness when deployed. In addition, the number of frame-modules can be flexibly adjusted according to the needs of different power.

The clearance joints of multi-module strut-mechanism have significant impact on constraints, number of degrees of freedom and topological structure of deployable system, which lead to the deviation between the actual movement and the ideal movement, increase dynamic stress of components, cause vibration and shock of assemblies, accelerate the abrasion of mechanism, and result in reduced accuracy of movement [3–5]. Therefore, carrying out dynamic analysis of deployable strut-mechanism with clearance joints is very important. Dynamic analysis of deployment and the influence law of joint clearance are the keys to master the movement characteristics of every joint and important components for multi-module deployable strut-mechanism, and the basis for optimization and the detailed design of deployment mechanism.

A.L. Adler from U.S. Air Force Research Laboratory conducted a preliminary dynamic analysis of the multi-module strut-mechanism, and analyzed the natural frequency and mode shapes under the action of gravity and different boundary conditions. In this paper, the result that the

✉ Shuli Yang
1034241127@qq.com

[1] Institute of Spacecraft System Engineering, China Academy of Space Technology, Beijing, China

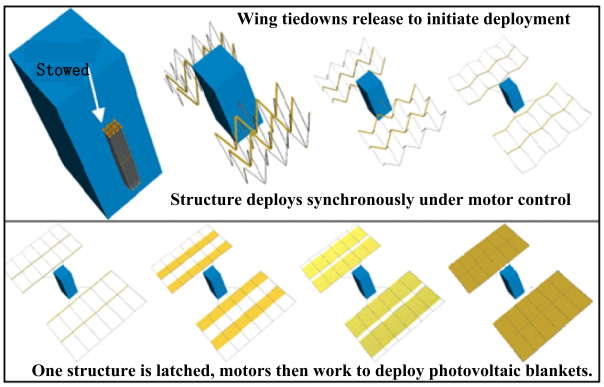

Fig. 1 Multi-module deployment of deployable strut-mechanism for solar array

hinge clearance has a certain influence on the strut deployment process has been pointed out, but impact analysis has not been performed [6]. M. Eskenazi from American ABLE Engineering Research Institute used finite element method to analyze the natural frequency and deformation of the multi-module strut-mechanism with different number of modules and different deployment configurations [7]. However, the references [6, 7] has not been carried out the dynamic analysis of the deployable process of the strut-mechanism, and has not been considered the influence of hinge clearance on the dynamic characteristics for strut-mechanism with multiple degrees of freedom.

In this paper, the multi-module dynamic models of deployable struts are established with considering the clearance root-joint by Kane dynamics theory. The deployable mode and process of strut-mechanism are researched. The dynamic characteristics of every joint and important components for multi-module deployable strut-mechanism and the influence law of joint clearance are analyzed and simulated, which provide the basis for the design of deployment mechanism.

2 The Components of Multi-module Deployable Strut-Mechanism

Multi-module deployable strut-mechanism after unfolded becomes a large-area and modular configuration composed of several struts, shown in Fig. 1; then the flexible blanket unfolds (shown in Fig. 2) within each rectangular bay, which form a large-area, flexible solar array generating high power. The deployment mode is the same within each standard module for multi-module deployable strut-mechanism. Multi-module deployable strut-mechanism has the advantages of low weight, high stiffness, low stowed volume, etc. The standard number of modules can be increased or decreased according to the needs, which can be satisfied the power requirements of different spacecraft missions [5].

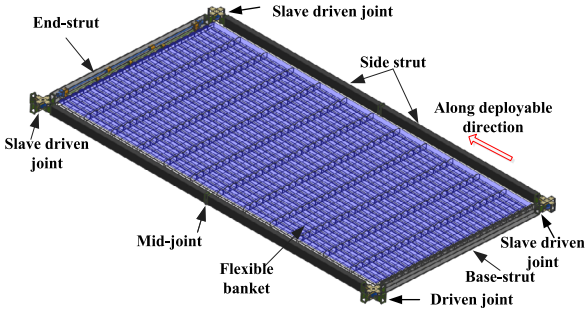

Fig. 2 Module of deployable strut-mechanism for solar array

Figure 2 shows the state of the fully deployment for a single-module deployable strut-mechanism. Base-strut, end strut and side strut are the main bearing units of solar array, generally made of carbon fiber–epoxy composites. Side struts are composed of two struts. Four side struts, one base-strut, one end strut constitute one regular bay, which is one of the modules of multi-module deployable strut-mechanism. The connection joints of base-strut, end strut and side strut are called driven units or slave driven units. Driven units provide power by a motor. Slave driven units don't have a motor, but contain the lock-buffer mechanism. The connection joints of two side struts are called intermediate hinge units.

3 The Dynamic Modeling of Deployable Strut-Mechanism Considering Clearance Root-Joint

A. The model of clearance root-joint

The dynamic models of deployable mechanism considering clearance root-joint are established based on Hertz contact theory [8] and Kane method. The important step in building joint-clearance mechanical models is setting up the relationship between the contact force and deformation. The contact configuration between the hinge pin and the bearing bush for root-joint is shown in Fig. 3. Given that the elastic modulus of the hinge pin is E_1, Poisson's ratio is ν_1, the radius is R_1; and the elastic modulus of the bearing bush is E_2, Poisson's ratio is ν_2, the radius is R_2. Dubowsky improved the Hertz contact law and proposed the nonlinear relationship between normal contact force F_N and deformation δ:

$$\delta = \frac{(k_1 + k_2)}{2a}\left[\ln\left(\frac{8a^3}{F_N R(k_1 + k_2)}\right) + 1\right]F_N. \tag{1}$$

Above formula R, k_1 and k_2 are separately:

$$R = \frac{R_1 R_2}{R_1 + R_2},\quad k_1 = \frac{1 - \nu_1^2}{\pi E_1},\quad k_2 = \frac{1 - \nu_2^2}{\pi E_2}. \tag{2}$$

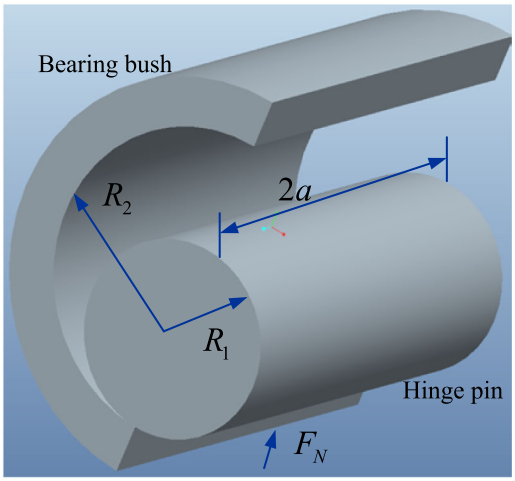

Fig. 3 Area-contact model between two cylinders

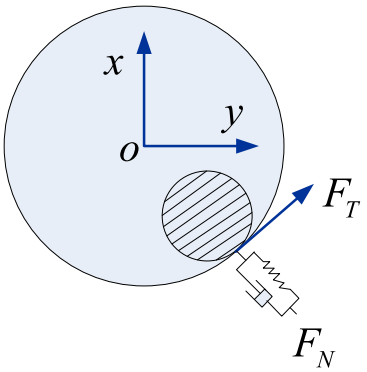

Fig. 4 Mechanical model of revolute joint with clearance

The formula (1) is dealt with nonlinearly and considers the damping effect. The expression of the contact force [9] can be written as

$$F_N = K\delta^n + D\dot{\delta} \tag{3}$$

The above formula K k is the linear contact stiffness coefficient; D is the damping coefficient; $\dot{\delta}$ is the contact velocity. The exponent n is generally 1.5 for the metal contact.

According to Coulomb friction law, the friction of the hinge pin at the contact points F_T is

$$F_\mathrm{T} = -\frac{v_\mathrm{T}}{|v_\mathrm{T}|}\mu F_\mathrm{N}, \tag{4}$$

where v_T is the tangential velocity of the hinge pin relative to the bearing bush at contact points; μ is the Coulomb friction coefficient.

The joint-clearance mechanical model by Hertz contact law and Coulomb friction law is shown in Fig. 4. *O-xy* coordinate system is established in the bearing bush. Given that

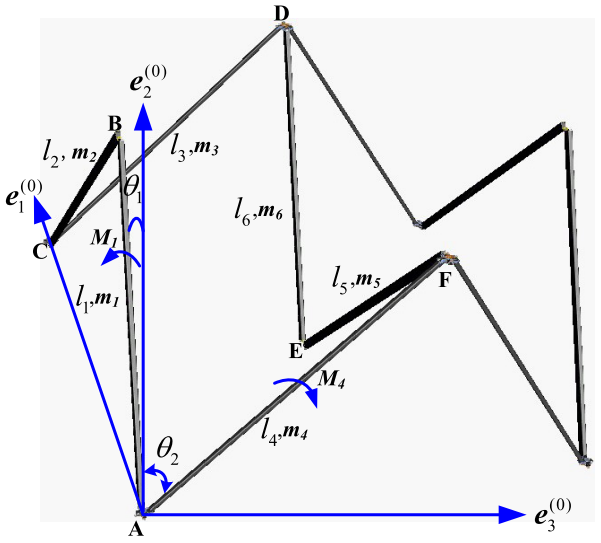

Fig. 5 Sketch of strut-mechanism's forces and moments

the center coordinate of the hinge pin is $(x_1,\ y_1)$; The clearance between hinge pin and bearing bush is $c = R_2 - R_1$; The contact deformation is $\delta = \sqrt{x_1^2 + y_1^2} - c$. Therefore, the contact force and friction can be expressed as follows:

$$\begin{aligned} F_\mathrm{N} &= \left(K\delta^n + D\dot{\delta}\right)S(\delta) \\ F_\mathrm{T} &= -\frac{v_\mathrm{T}}{|v_\mathrm{T}|}\mu F_\mathrm{N} S(\delta) \end{aligned} \quad S(\delta) = \begin{cases} 1 & \delta > 0 \\ 0 & \delta \le 0 \end{cases}. \tag{5}$$

B. The dynamic models of deployable strut-mechanism based on Kane method

(1) The definition of the system of generalized coordinates

Unit vectors of three directions in Cartesian coordinates are indicated separately with $e_1^{(0)}, e_2^{(0)}, e_3^{(0)}$, as shown in Fig. 5. The degrees of freedom for the system are 6, which x_{01}, y_{01}, y_{02}, z_{02}, θ_1, θ_2 are chosen as generalized coordinates.

(2) The kinematic analysis of deployable strut-mechanism

In this paper, the clearance influence of the rotating hinge including AB strut rotating around A point and AF strut rotating around A point are separately considered, as shown in Fig. 6.

The displacement, velocity and acceleration of each strut are expressed as functions of the generalized coordinates. In Fig. 6, the external forces contain inertia forces and moments of inertia. To obtain inertia force and moment of inertia, the relationships among the displacement, velocity, acceleration of each strut's centroid and generalized coordinates should be determined first. Given that the displacement and angular displacement vectors of each strut's centroid are separately expressed as $\boldsymbol{L}_i$, $\boldsymbol{\theta}_i$, $(i = 1, 2, 3, 4, 5, 6)$; the velocity and angular velocity vectors of each strut's centroid are separately expressed as $\boldsymbol{V}_{ci}$, $\boldsymbol{\omega}_i$, $(i = 1, 2, 3, 4, 5, 6)$; the acceleration

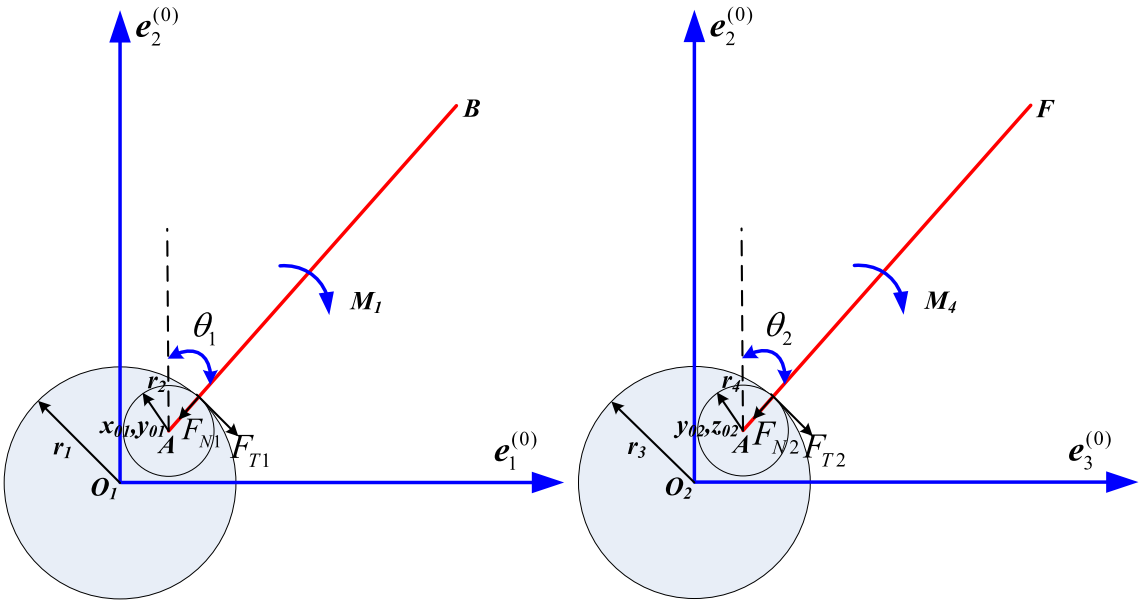

Fig. 6 AB strut and AF strut with clearance joint

and angular acceleration vectors of each strut's centroid are separately expressed as $\boldsymbol{a}_{ci}$, $\boldsymbol{\varepsilon}_i$, $(i = 1, 2, 3, 4, 5, 6)$; and the moments of inertia of each strut around centroid are separately expressed as J_i, $(i = 1, 2, 3, 4, 5, 6)$.

(a) The Calculation of the Strut's Displacement $\boldsymbol{L}_i$

Given that the generalized speed is derivative of generalized coordinate, so there are $u_{x01} = \dot{x}_{01}$, $u_{y01} = \dot{y}_{01}$, $u_{y02} = \dot{y}_{02}$, $u_{z02} = \dot{z}_{02}$, $u_1 = \dot{\theta}_1$, $u_2 = \dot{\theta}_2$.

By taking the derivative of $\boldsymbol{L}_i$ with respect to time, the centroid velocity and the angular velocity of each strut are obtained as follows:

$$
\begin{cases}
\boldsymbol{L}_1 = (x_{01} + l_1/2\sin\theta_1)\boldsymbol{e}_1^{(0)} + (y_{01} + l_1/2\cos\theta_1)\boldsymbol{e}_2^{(0)} \\
\boldsymbol{\theta}_1 = -\theta_1\boldsymbol{e}_3^{(0)} \\
\boldsymbol{L}_2 = (x_{01} + (l_1 + l_2/2)\sin\theta_1)\boldsymbol{e}_1^{(0)} + (y_{01} + l_2/2\cos\theta_1)\boldsymbol{e}_2^{(0)} \\
\boldsymbol{\theta}_2 = \theta_1\boldsymbol{e}_3^{(0)} \\
\boldsymbol{L}_3 = (x_{01} + (l_1 + l_2)\sin\theta_1)\boldsymbol{e}_1^{(0)} + \left(y_{02} + \dfrac{l_3}{2\cos\theta_2}\right)\boldsymbol{e}_2^{(0)} + (z_{02} + l_3/2\sin\theta_2)\boldsymbol{e}_3^{(0)} \\
\boldsymbol{\theta}_3 = \theta_2\boldsymbol{e}_1^{(0)} \\
\boldsymbol{L}_4 = (y_{02} + l_4/2\cos\theta_2)\boldsymbol{e}_2^{(0)} + (z_{02} + l_4/2\sin\theta_2)\boldsymbol{e}_3^{(0)} \\
\boldsymbol{\theta}_4 = \theta_2\boldsymbol{e}_1^{(0)} \\
\boldsymbol{L}_5 = (x_{01} + l_5/2\sin\theta_1)\boldsymbol{e}_1^{(0)} + (y_{01} + l_5/2\cos\theta_1)\boldsymbol{e}_2^{(0)} + (z_{02} + l_4\sin\theta_2)\boldsymbol{e}_3^{(0)} \\
\boldsymbol{\theta}_5 = \theta_1\boldsymbol{e}_3^{(0)} \\
\boldsymbol{L}_6 = (x_{01} + (l_5 + l_6/2)\sin\theta_1)\boldsymbol{e}_1^{(0)} + \left(y_{01} + \dfrac{l_6}{2\cos\theta_1}\right)\boldsymbol{e}_2^{(0)} + (z_{02} + l_4\sin\theta_2)\boldsymbol{e}_3^{(0)} \\
\boldsymbol{\theta}_6 = -\theta_1\boldsymbol{e}_3^{(0)}
\end{cases}
$$

$$\begin{cases} \boldsymbol{V}_{ci} = \dfrac{\mathrm{d}\boldsymbol{L}_i}{\mathrm{d}t} \\ \boldsymbol{\omega}_i = \dfrac{\mathrm{d}\boldsymbol{\theta}_i}{\mathrm{d}t} \end{cases} \quad (i = 1, 2, 3, 4, 5, 6). \tag{6}$$

By taking the derivative of velocity and angular velocity with respect to time, the centroid acceleration and angular acceleration of each strut are obtained as follows:

$$\begin{cases} \boldsymbol{a}_{ci} = \dfrac{\mathrm{d}^2\boldsymbol{L}_i}{\mathrm{d}t^2} = \dfrac{\mathrm{d}\boldsymbol{V}_{ci}}{dt^2} \\ \boldsymbol{\varepsilon}_{ci} = \dfrac{\mathrm{d}^2\boldsymbol{\theta}_i}{\mathrm{d}t^2} = \dfrac{\mathrm{d}\boldsymbol{\omega}_i}{\mathrm{d}t^2} \end{cases} \quad (i = 1, 2, 3, 4, 5, 6). \tag{7}$$

(b) Active forces and inertia forces of struts

Due to the root-joint clearance, the hinge pin of AB and AF strut generates active forces from the bearing bush, which contain friction and contact forces. Therefore, the active forces effecting on AB strut include driven torque $\boldsymbol{M}_1$, friction $\boldsymbol{F}_{N1}$ and contact forces $\boldsymbol{F}_{T1}$ of hinge pin; and the active forces effecting on AF strut include driven torque $\boldsymbol{M}_4$, friction $\boldsymbol{F}_{N2}$ and contact forces $\boldsymbol{F}_{T2}$ of hinge pin. The radius of the bearing bush and hinge pin are separately defined as r_1, r_2 for A rotating point of AB strut; and the radius of the bearing bush and hinge pin are separately defined as r_3, r_4 for A rotating point of AF strut. Given that contact stiffness, stiffness and friction coefficient of the rotating hinge for AB strut are separately defined as K_1, D_1, μ_1; and contact stiffness, stiffness and friction coefficient of the rotating hinge for AF strut are separately defined as K_2, D_2, μ_2:

$$\begin{aligned} \delta_1 &= \sqrt{x_{01}^2 + y_{01}^2} - (r_1 - r_2) \\ F_{N1} &= \left(K_1\delta_1 + D_1\dot{\delta}_1\right)S(\delta_1) \\ &= \left\{K_1\left(\sqrt{x_{01}^2 + y_{01}^2} - (r_1 - r_2)\right) + D_1\frac{x_{01}\dot{x}_{01} + y_{01}\dot{y}_{01}}{\sqrt{x_{01}^2 + y_{01}^2}}\right\}S(\delta_1) \\ F_{T1} &= -\frac{v_{T1}}{|v_{T1}|}\mu_1 F_{N1}S(\delta_1) \\ \delta_2 &= \sqrt{y_{02}^2 + z_{02}^2} - (r_3 - r_4) \\ F_{N2} &= \left(K_2\delta_2 + D_2\dot{\delta}_2\right)S(\delta_2) \\ &= \left\{K_2\left(\sqrt{y_{02}^2 + z_{02}^2} - (r_3 - r_4)\right) + D_2\frac{y_{02}\dot{y}_{02} + z_{02}\dot{z}_{02}}{\sqrt{y_{02}^2 + z_{02}^2}}\right\}S(\delta_2) \\ F_{T2} &= -\frac{v_{T2}}{|v_{T2}|}\mu_2 F_{N2}S(\delta_2). \end{aligned}$$

Active torques are as follows:

$$\begin{aligned} \boldsymbol{F}_{N1} &= -F_{N1}\frac{x_{01}}{\sqrt{x_{01}^2 + y_{01}^2}}\boldsymbol{e}_1^{(0)} - F_{N1}\frac{y_{01}}{\sqrt{x_{01}^2 + y_{01}^2}}\boldsymbol{e}_2^{(0)} \\ \boldsymbol{M}_{T1} &= -F_{T1}r_2\boldsymbol{e}_3^{(0)},\ \boldsymbol{M}_1 = -M_1\boldsymbol{e}_3^{(0)} \\ \boldsymbol{F}_{N2} &= -F_{N2}\frac{y_{02}}{\sqrt{y_{02}^2 + z_{02}^2}}\boldsymbol{e}_2^{(0)} - F_{N2}\frac{z_{02}}{\sqrt{y_{02}^2 + z_{02}^2}}\boldsymbol{e}_3^{(0)} \\ \boldsymbol{M}_{T2} &= F_{T2}r_4\boldsymbol{e}_1^{(0)},\ \boldsymbol{M}_4 = M_4\boldsymbol{e}_1^{(0)}. \end{aligned}$$

Moments of inertia are as follows:

$$\boldsymbol{F}_i^* = -m_i\boldsymbol{a}_{ci},\ \boldsymbol{M}_i^* = -J_i\boldsymbol{\varepsilon}_i\ (i = 1, 2, 3, 4, 5, 6) \tag{8}$$

(c) Generalized active forces and generalized inertial forces

The partial velocities constitute a transformation matrix, which are the partial differential of the centroid velocity and angular velocity with respect to generalized velocity. Then the matrix multiplying by force vector can obtain the generalized forces:

$$\boldsymbol{U}_F = \begin{pmatrix} \frac{\partial\boldsymbol{V}_{c1}}{\partial u_1} & \frac{\partial\boldsymbol{V}_{c2}}{\partial u_1} & \frac{\partial\boldsymbol{V}_{c3}}{\partial u_1} & \frac{\partial\boldsymbol{V}_{c4}}{\partial u_1} & \frac{\partial\boldsymbol{V}_{c5}}{\partial u_1} & \frac{\partial\boldsymbol{V}_{c6}}{\partial u_1} \\ \frac{\partial\boldsymbol{V}_{c1}}{\partial u_2} & \frac{\partial\boldsymbol{V}_{c2}}{\partial u_2} & \frac{\partial\boldsymbol{V}_{c3}}{\partial u_2} & \frac{\partial\boldsymbol{V}_{c4}}{\partial u_2} & \frac{\partial\boldsymbol{V}_{c5}}{\partial u_2} & \frac{\partial\boldsymbol{V}_{c6}}{\partial u_2} \\ \frac{\partial\boldsymbol{V}_{c1}}{\partial u_{x01}} & \frac{\partial\boldsymbol{V}_{c2}}{\partial u_{x01}} & \frac{\partial\boldsymbol{V}_{c3}}{\partial u_{x01}} & \frac{\partial\boldsymbol{V}_{c4}}{\partial u_{x01}} & \frac{\partial\boldsymbol{V}_{c5}}{\partial u_{x01}} & \frac{\partial\boldsymbol{V}_{c6}}{\partial u_{x01}} \\ \frac{\partial\boldsymbol{V}_{c1}}{\partial u_{y01}} & \frac{\partial\boldsymbol{V}_{c2}}{\partial u_{y01}} & \frac{\partial\boldsymbol{V}_{c3}}{\partial u_{y01}} & \frac{\partial\boldsymbol{V}_{c4}}{\partial u_{y01}} & \frac{\partial\boldsymbol{V}_{c5}}{\partial u_{y01}} & \frac{\partial\boldsymbol{V}_{c6}}{\partial u_{y01}} \\ \frac{\partial\boldsymbol{V}_{c1}}{\partial u_{y02}} & \frac{\partial\boldsymbol{V}_{c2}}{\partial u_{y02}} & \frac{\partial\boldsymbol{V}_{c3}}{\partial u_{y02}} & \frac{\partial\boldsymbol{V}_{c4}}{\partial u_{y02}} & \frac{\partial\boldsymbol{V}_{c5}}{\partial u_{y02}} & \frac{\partial\boldsymbol{V}_{c6}}{\partial u_{y02}} \\ \frac{\partial\boldsymbol{V}_{c1}}{\partial u_{z02}} & \frac{\partial\boldsymbol{V}_{c2}}{\partial u_{z02}} & \frac{\partial\boldsymbol{V}_{c3}}{\partial u_{z02}} & \frac{\partial\boldsymbol{V}_{c4}}{\partial u_{z02}} & \frac{\partial\boldsymbol{V}_{c5}}{\partial u_{z02}} & \frac{\partial\boldsymbol{V}_{c6}}{\partial u_{z02}} \end{pmatrix}$$

$$\boldsymbol{U}_M = \begin{pmatrix} \frac{\partial\boldsymbol{\omega}_1}{\partial u_1} & \frac{\partial\boldsymbol{\omega}_2}{\partial u_1} & \frac{\partial\boldsymbol{\omega}_3}{\partial u_1} & \frac{\partial\boldsymbol{\omega}_4}{\partial u_1} & \frac{\partial\boldsymbol{\omega}_5}{\partial u_1} & \frac{\partial\boldsymbol{\omega}_6}{\partial u_1} \\ \frac{\partial\boldsymbol{\omega}_1}{\partial u_2} & \frac{\partial\boldsymbol{\omega}_2}{\partial u_2} & \frac{\partial\boldsymbol{\omega}_3}{\partial u_2} & \frac{\partial\boldsymbol{\omega}_4}{\partial u_2} & \frac{\partial\boldsymbol{\omega}_5}{\partial u_2} & \frac{\partial\boldsymbol{\omega}_6}{\partial u_2} \\ \frac{\partial\boldsymbol{\omega}_1}{\partial u_{x01}} & \frac{\partial\boldsymbol{\omega}_2}{\partial u_{x01}} & \frac{\partial\boldsymbol{\omega}_3}{\partial u_{x01}} & \frac{\partial\boldsymbol{\omega}_4}{\partial u_{x01}} & \frac{\partial\boldsymbol{\omega}_5}{\partial u_{x01}} & \frac{\partial\boldsymbol{\omega}_6}{\partial u_{x01}} \\ \frac{\partial\boldsymbol{\omega}_1}{\partial u_{y01}} & \frac{\partial\boldsymbol{\omega}_2}{\partial u_{y01}} & \frac{\partial\boldsymbol{\omega}_3}{\partial u_{y01}} & \frac{\partial\boldsymbol{\omega}_4}{\partial u_{y01}} & \frac{\partial\boldsymbol{\omega}_5}{\partial u_{y01}} & \frac{\partial\boldsymbol{\omega}_6}{\partial u_{y01}} \\ \frac{\partial\boldsymbol{\omega}_1}{\partial u_{y02}} & \frac{\partial\boldsymbol{\omega}_2}{\partial u_{y02}} & \frac{\partial\boldsymbol{\omega}_3}{\partial u_{y02}} & \frac{\partial\boldsymbol{\omega}_4}{\partial u_{y02}} & \frac{\partial\boldsymbol{\omega}_5}{\partial u_{y02}} & \frac{\partial\boldsymbol{\omega}_6}{\partial u_{y02}} \\ \frac{\partial\boldsymbol{\omega}_1}{\partial u_{z02}} & \frac{\partial\boldsymbol{\omega}_2}{\partial u_{z02}} & \frac{\partial\boldsymbol{\omega}_3}{\partial u_{z02}} & \frac{\partial\boldsymbol{\omega}_4}{\partial u_{z02}} & \frac{\partial\boldsymbol{\omega}_5}{\partial u_{z02}} & \frac{\partial\boldsymbol{\omega}_6}{\partial u_{z02}} \end{pmatrix}$$

Generalized active forces are as follows:

$$\begin{aligned} \boldsymbol{F} &= \boldsymbol{U}_F[\boldsymbol{F}_{N1},\ 0,\ 0,\ \boldsymbol{F}_{N2},\ 0,\ 0]^{\mathrm{T}} \\ &\quad + \boldsymbol{U}_M[\boldsymbol{M}_1 + \boldsymbol{M}_{T1},\ 0,\ 0,\ \boldsymbol{M}_4 + \boldsymbol{M}_{T2},\ 0,\ 0]^{\mathrm{T}}. \end{aligned} \tag{9}$$

Generalized inertial forces are as follows:

$$\begin{aligned} \boldsymbol{F}^* &= \boldsymbol{U}_F[\boldsymbol{F}_1^*,\ \boldsymbol{F}_2^*,\ \boldsymbol{F}_3^*,\ \boldsymbol{F}_4^*,\ \boldsymbol{F}_5^*,\ \boldsymbol{F}_6^*]^{\mathrm{T}} \\ &\quad + \boldsymbol{U}_M[\boldsymbol{M}_1^*,\ \boldsymbol{M}_2^*,\ \boldsymbol{M}_3^*,\ \boldsymbol{M}_4^*,\ \boldsymbol{M}_5^*,\ \boldsymbol{M}_6^*]^{\mathrm{T}}. \end{aligned} \tag{10}$$

Dynamic equation of strut is represented as follows:

$$\boldsymbol{F} + \boldsymbol{F}^* = 0 \tag{11}$$

Dynamic equations of struts are represented as follows:

$$\begin{aligned} &\left(-m_1\frac{l_1}{2} - m_2\left(l_1 + \frac{l_2}{2}\right) - m_3(l_1 + l_2) - m_5\frac{l_5}{2}\right. \\ &\left.-m_6\left(l_5 + \frac{l_6}{2}\right)\right)\cos\theta_1\dot{u}_{x01} + \left(m_1\frac{l_1}{2} + m_2\frac{l_2}{2} + m_5\frac{l_5}{2} + m_6\frac{l_6}{2}\right)\sin\theta_1\dot{u}_{y01} \end{aligned}$$

$$
\begin{aligned}
&-\left(m_1\frac{l_1^2}{4}+m_2\frac{l_2^2}{4}+m_5\frac{l_5^2}{4}+m_6\frac{l_6^2}{4}\right)\dot{u}_1\\
&-\left(m_2\left(l_1^2+l_1l_2\right)+m_3(l_1+l_2)^2+m_6\left(l_5^2+l_5l_6\right)\right)\\
&\left(\dot{u}_1\cos^2\theta_1-u_1^2\sin\theta_1\cos\theta_1\right)-(J_1+J_2+J_5+J_6)\dot{u}_1\\
&-\frac{l_1}{2}F_{N1}\left(\cos\theta_1\frac{x_{01}}{\sqrt{x_{01}^2+y_{01}^2}}+\sin\theta_1\frac{y_{01}}{\sqrt{x_{01}^2+y_{01}^2}}\right)+M_1+F_{T1}r_2=0.
\end{aligned}
\tag{12}
$$

$$
\begin{aligned}
&-(m_3+m_4)\,\dot{u}_{y02}\\
&+\left(m_3\frac{l_3}{2}+m_4\frac{l_4}{2}\right)\left(\dot{u}_2\sin\theta_2+u_2^2\cos\theta_2\right)\\
&-F_{N2}\frac{y_{02}}{\sqrt{y_{02}^2+z_{02}^2}}=0
\end{aligned}
\tag{13}
$$

$$
\begin{aligned}
&\left(m_3\frac{l_3}{2}+m_4\frac{l_4}{2}\right)\sin\theta_2\dot{u}_{y02}\\
&-\left(m_3\frac{l_3}{2}+m_4\frac{l_4}{2}+m_5l_4+m_6l_4\right)\cos\theta_2\dot{u}_{z02}\\
&-\left(m_3\frac{l_3^2}{4}+m_4\frac{l_4^2}{4}\right)\dot{u}_2\\
&-(m_5+m_6)\,l_4^2\left(\dot{u}_2\cos^2\theta_2-u_2^2\sin\theta_2\cos\theta_2\right)\\
&-(J_3+J_4)\,\dot{u}_2\\
&+\frac{l_4}{2}F_{N2}\left(\sin\theta_2\frac{y_{02}}{\sqrt{y_{02}^2+z_{02}^2}}+\cos\theta_2\frac{z_{02}}{\sqrt{y_{02}^2+z_{02}^2}}\right)\\
&+M_4+F_{T2}r_4=0.
\end{aligned}
\tag{14}
$$

$$
\begin{aligned}
&-(m_1+m_2+m_5+m_6)\dot{u}_{y01}\\
&+\left(m_1\frac{l_1}{2}+m_2\frac{l_2}{2}+m_5\frac{l_5}{2}+m_6\frac{l_6}{2}\right)\left(\dot{u}_1\sin\theta_1+u_1^2\cos\theta_1\right)\\
&-F_{N1}\frac{y_{01}}{\sqrt{x_{01}^2+y_{01}^2}}=0.
\end{aligned}
\tag{15}
$$

$$
\begin{aligned}
&-(m_1+m_2+m_3+m_5+m_6)\dot{u}_{x01}\\
&-\left(m_1\frac{l_1}{2}+m_2\left(l_1+\frac{l_2}{2}\right)+m_3(l_1+l_2)+m_5\frac{l_5}{2}+m_6\left(l_5+\frac{l_6}{2}\right)\right)\\
&\left(\dot{u}_1\cos\theta_1-u_1^2\sin\theta_1\right)-F_{N1}\frac{x_{01}}{\sqrt{x_{01}^2+y_{01}^2}}=0
\end{aligned}
\tag{16}
$$

$$
\begin{aligned}
&-(m_3+m_4+m_5+m_6)\,\dot{u}_{z02}\\
&-\left(m_3\frac{l_3}{2}+m_4\frac{l_4}{2}+m_5l_4+m_6l_4\right)\left(\dot{u}_2\cos\theta_2+u_2^2\sin\theta_2\right)\\
&-F_{N2}\frac{z_{02}}{\sqrt{y_{02}^2+z_{02}^2}}=0.
\end{aligned}
\tag{17}
$$

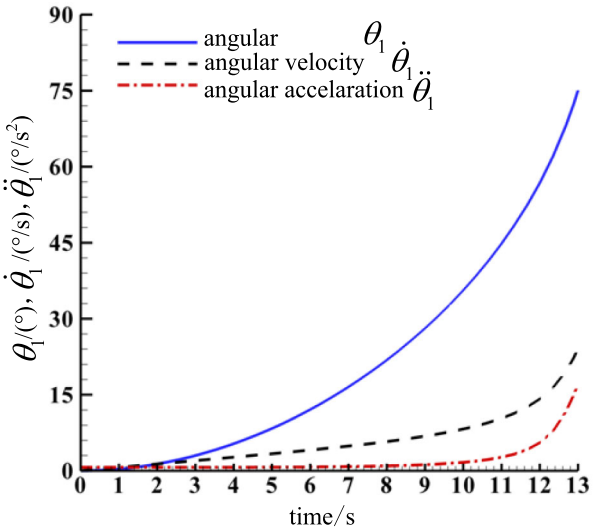

Fig. 7 θ_1, $\dot{\theta}_1$, $\ddot{\theta}_1$ of AB strut

4 Results of Dynamic Analysis of Deployable Strut-Mechanism

According to the dynamic equations of deployable strut-mechanism, the numerical solutions of dynamic parameters are obtained by making use of the classic fourth-order Runge–Kutta method. In this case the input parameters used in calculations are shown in Table 1.

A. Dynamic analysis of deployable strut-mechanism without considering clearance root-joint

The dynamic responses of parameters of deployable strut-mechanism without considering clearance root-joint, such as the rotating angle of AB strut θ_1, the rotating angle of AF strut θ_2 are shown in Figs. 7 and 8.

(a) Time-dependence of θ_1, $\dot{\theta}_1$, $\ddot{\theta}_1$ *for AB strut*

(b) Time-dependence of θ_2, $\dot{\theta}_2$, $\ddot{\theta}_2$ for AF strut

Figures 7 and 8 show:

(1) θ_1, $\dot{\theta}_1$, $\ddot{\theta}_1$ and θ_2, $\dot{\theta}_2$, $\ddot{\theta}_2$ increase with time. However, $\ddot{\theta}_1$ and $\ddot{\theta}_2$ increase slowly with time, the trend of which is not obvious;
(2) When $M_1 = 1.0$, $M_4 = 0.3$, θ_1 θ_2 can rotate 90° simultaneously after 13.5 s. And then, the angle of AB strut and AF strut is 90° in the *xoz* plane.

B. Dynamic analysis of deployable strut-mechanism with considering clearance root-joint

Table 1 Parameters of deployable strut-mechanism for dynamic analysis

Index	Parameters	Symbol	Unit	Value
1.	Strut length	l_i, $(i = 1, 2, 3, 4, 5, 6)$	m	2.5
2.	density	ρ_i, $(i = 1, 2, 3, 4, 5, 6)$	kg/m^2	7800
3.	Moment of AB strut	M_1	N.m	1
4.	Moment of AF strut	M_4	N.m	0.3
5.	Radius of strut	r_i', $(i = 1, 2, 3, 4, 5, 6)$	m	0.005
6.	Radius of AB strut's bearing bush	r_1	m	0.005
7.	Radius of AB strut's hinge pin	r_2	m	0.0049
8.	Radius of AF strut's bearing bush	r_3	m	0.005
9.	Radius of AF strut's hinge pin	r_4	m	0.0049
10.	Stiffness coefficient	K_1	N.m	10,000,000
11.	Stiffness coefficient	K_2	N.m	10,000,000
12.	Damping coefficient	D_1	N.s/m	178.7
13.	Damping coefficient	D_2	N.s/m	178.7
14.	Dynamic friction coefficient	μ_1	/	0.1
15.	Dynamic friction coefficient	μ_2	/	0.1
16.	Moment of inertia of the centroid	J_i, $(i = 1, 2, 3, 4, 5, 6)$	kg.m^2	0.000019144

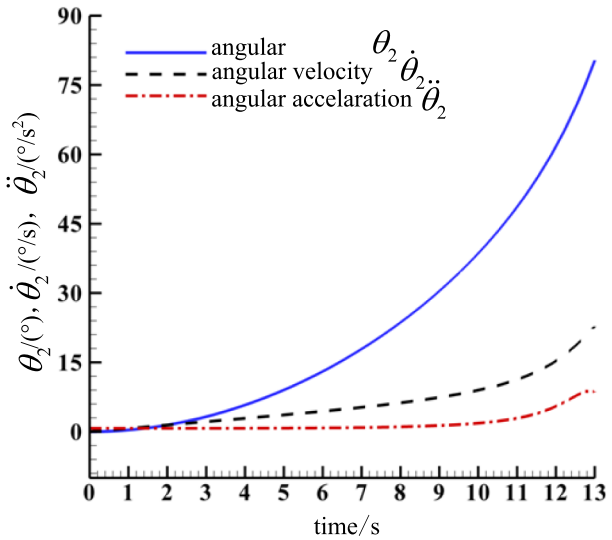

Fig. 8 θ_2, $\dot{\theta}_2$, $\ddot{\theta}_2$ of AF strut

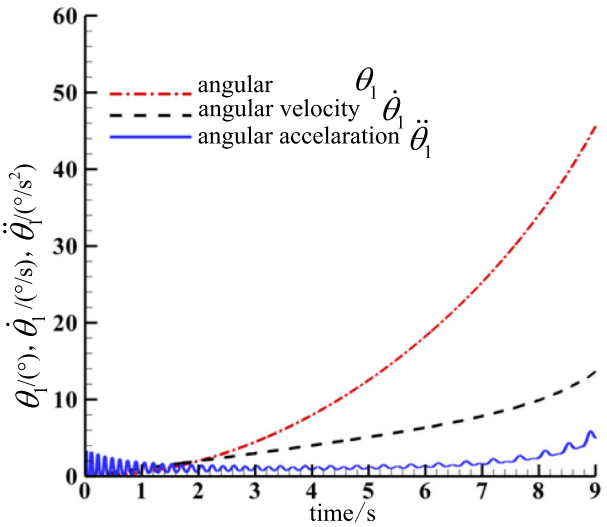

Fig. 9 θ_1, $\dot{\theta}_1$, $\ddot{\theta}_1$ of AB strut

The dynamic responses of parameters of deployable strut-mechanism with considering clearance root-joint such as the rotating angle of AB strut θ_1, the x direction of B point of AB strut, x_{01}, y_{01}, F_{N1} and F_{N2} are shown in Figures 9, 10, 11, 12, 13 and 14. The initial values of x_{01}, y_{01} are separately 0–0.0001 m; and the initial values of y_{02}, z_{02} are separately − 0.0001 m, 0 m.

(a) Time-dependence of θ_1, $\dot{\theta}_1$, $\ddot{\theta}_1$

(b) Time-dependence of x_{01}, y_{01}

(c) Time-dependence of F_{N1}

(d) Time-dependence of θ_2, $\dot{\theta}_2$, $\ddot{\theta}_2$

(e) Time-dependence of F_{N2}

Figures 9, 10, 11, 12, 13 and 14 show:

(1) Root-joint clearance has almost no influence on the time-dependence of $\dot{\theta}_1$and and θ_2, $\dot{\theta}_2$, but to some extent effect on the time-dependence of $\ddot{\theta}_1$ and $\ddot{\theta}_2$. Amplitude

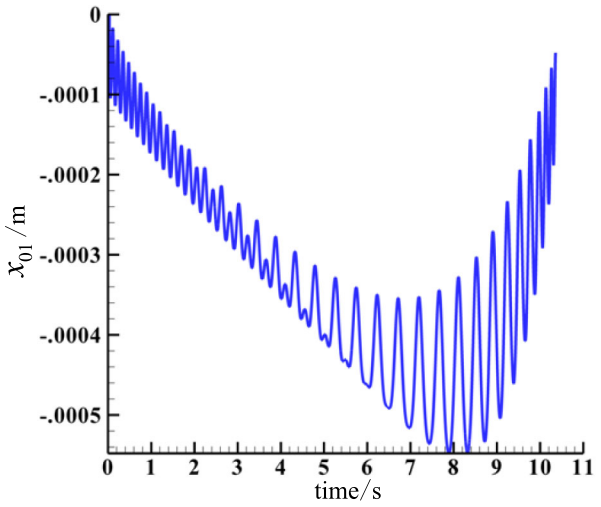

Fig. 10 x_{01} of A point's revolute joint with clearance on AB strut

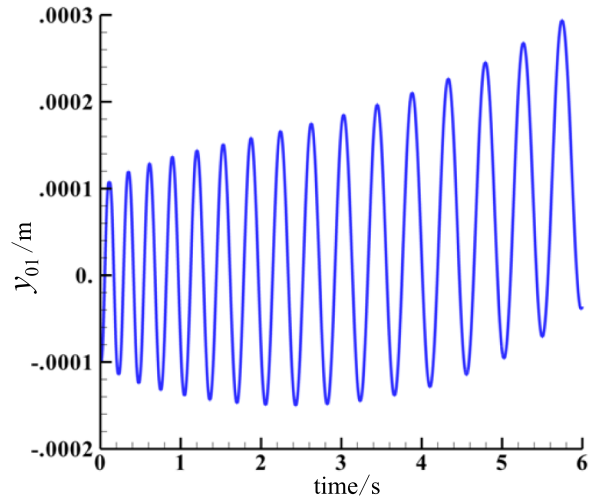

Fig. 11 y_{01} of A point's revolute joint with clearance on AB strut

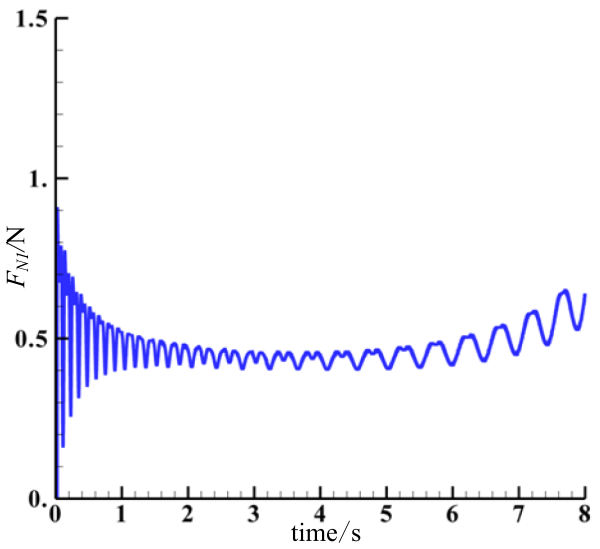

Fig. 12 F_{N1} of A point's revolute joint with clearance on AB strut

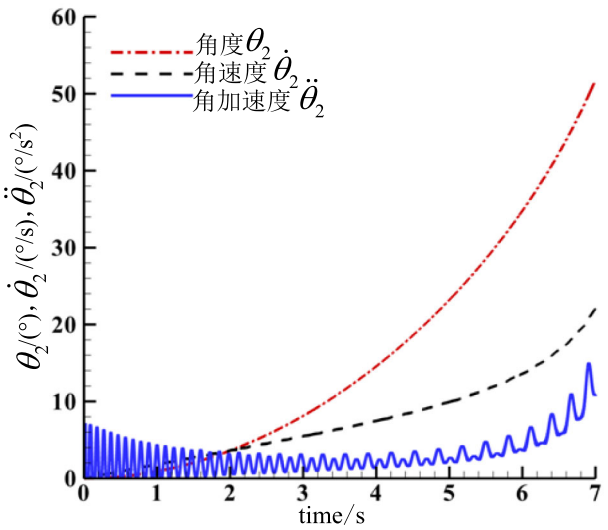

Fig. 13 θ_2, $\dot{\theta}_2$, $\ddot{\theta}_2$ of AF strut

of angular acceleration appears significant fluctuations in 0–2 s and stabilizes gradually, indicating the hinge pin in the bearing bush is in the state of constant contact and separation;

(2) In the interval of θ_1 rotated 90°, $|x_{01}|$ appears the trend of increasing first and then decreasing. The maximum of $|x_{01}|$ is 0.00054 m. $|y_{01}|$ varies within 0.0001 m. When $\theta_1 = 90°$, $|y_{01}|$ appears the trend of slightly increasing;

(3) F_{N1} and F_{N2} gradually stabilizes with time. The stabilized value of F_{N1} is about 0.48 N, and the stabilized value of F_{N2} is about 0.4 N;

(4) The deployable time appears different for strut-mechanism when considering and without considering clearance root-joint. AF strut can rotate 90° after 9 s with considering clearance root-joint. In addition, AF strut can rotate 90° after 13.5 s without considering clearance root-joint. Thus, the existence of clearance root-joint will lead to the different rotating degrees of θ_1 and θ_2 at the same time.

5 Conclusions

With Kane dynamics theory, the multi-body dynamic models of deployable struts have been established with considering the clearance root-joints, and the deployable style and deployable process of the struts have been studied. The conclusions are as follows:

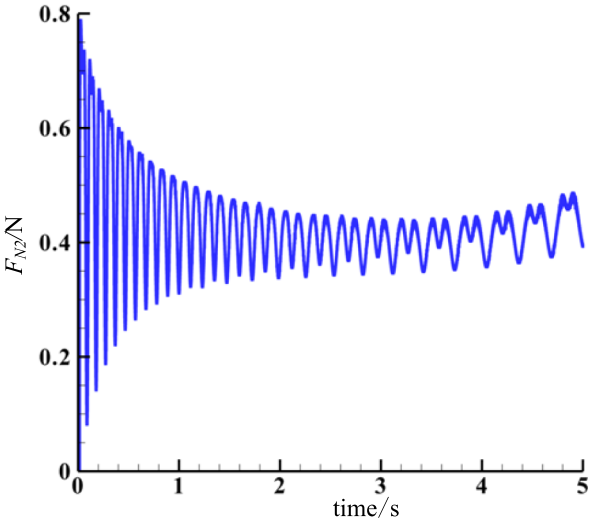

Fig. 14 T F_{N2} F_{N2} of A point's revolute joint with clearance on AF strut

(1) Root-joint clearance has almost no influence on the rotation angle and angular velocity of base-strut, but to some extent effect on the angular acceleration of base-strut. Amplitude of angular acceleration appears significant fluctuations in 0–2 s and stabilizes gradually, indicating the hinge pin in the bearing bush is in the state of constant contact and separation.

(2) The absolute value of the displacement in the X direction for the hinge pin connected to AB side-strut first increases then decreases in the period of AB strut rotating 90 degrees, which maximum value is 0.0005 m; and the displacement in the Y direction appears substantially sinusoidal trend, which is in the range of [− 0.0001 m, 0.0001 m], illustrating that the hinge pin has certain impact on the bearing bush in the process of deployable strut-mechanism.

(3) The value of the contact force F_{N1} for AB side-strut is gradually stabilized in 0.45 N considering root-joint clearance; and the value of the contact force F_{N2} for AF base-strut is gradually stabilized in 0.4 N. The reason why F_{N1} is larger is that the AB side-strut needs to rotate BC side-strut, meaning the joint of AB strut generating greater impact load.

(4) The dynamic models of deployable struts considering root-hinge clearance describe more actually the dynamic characteristics of system. The fluctuation of the angular acceleration and joint's impact in the deployable process because of joint clearance are amplified along with long dimension of solar array, giving rise to the larger tip displacement of the solar array, which have adverse effect on the structure. To this end, the clearance should be controlled.

(5) Based on the model of root-joint clearance, the driven moment should be analyzed to determine a reasonable ratio of $\boldsymbol{M}_1$ and $\boldsymbol{M}_4$.

Funding No external funding was used.

Declarations

Conflict of interest The authors declare that they have no competing interests.

Ethical approval All procedures performed in studies involving human participants were in accordance with the ethical standards of the institutional and/or national research committee and with the 1964 Helsinki declaration and its later amendments or comparable ethical standards.

References

1. Liu Z-q, Yang S-l, Pu H-l (2012) Development and trend of space solar array technology. Spacecr Eng 21(6):112–118
2. Botke M, Murphy D, Murphey T, et al (2002) Zero deadband, multiple strut synchronized hinge for deployable structures. In: Proceedings of the 36th Aerospace Mechanisms Symposium, Glenn Research Center, May 15–17, 2002
3. Wang G-x, Liu H-z (2015) Dynamics analysis of 4-SPS/CU parallel mechanism with spherical joint clearance. J Mech Eng 51 (1): 43–51
4. Li Y-b, Xu T-t et al (2020) Dynamic characteristics of spatial parallel mechanism with spherical joint clearance. J Zhejiang Univ (Engineering Science) 54(2):348–356
5. Wang W, Sun J, Yu D-y et al (2004) Analytical model for complex joint with latch mechanism of space structure. J Astronaut 25(1):1–5
6. Adler AL, Hague N, Spanjers G, et al (2003) Powersail-the challenges of large, planar, surface structures for space applications. In: 44th AIAA/ASME/ASCE/AHS/ASC Structures, Structural Dynamics, and Materials Conference, Norfolk, VA, April 7–10, 2003
7. Eskenazi M, White S, Spence B et al (2005) Promising results from three NASA SBIR solar array technology development programs. NASA/CP-2005-213431:59–94
8. Yang Z, Zheng-feng B, Xing-gui W (2010) Dynamics analysis of two-axis-position mechanism of satellite antennas with joint clearance. J Astronaut 31(6):1533–1539
9. Yang Z, Zheng FB (2011) Dynamics analysis of space robot manipulator with joint clearance. Acta Astronaut 68(7):1147–1155